EurJIC
European Journal of Inorganic Chemistry

Research Article
doi.org/10.1002/ejic.202200043

Chemistry Europe
European Chemical Societies Publishing

www.eurjic.org

Europium (II) Sulfate $EuSO_4$: Synthesis Methods, Crystal and Electronic Structure, Luminescence Properties

Yuriy G. Denisenko,*[a, b, c] Alexander E. Sedykh,[b] Aleksandr S. Oreshonkov,[d, e] Maxim S. Molokeev,[f, g, h] Nikita O. Azarapin,[c] Elena I. Sal'nikova,[c, i] Olga D. Chimitova,[j] Oleg V. Andreev,[c, k] Illaria A. Razumkova,[c] and Klaus Müller-Buschbaum[b, l]

In the present work, we report on the synthesis of $EuSO_4$ powders by two different methods using EuS as starting material. The compound $EuSO_4$ contains divalent europium and crystallizes in the orthorhombic crystal system, space group **P***nma* with parameters close to $SrSO_4$. The compound exhibits near isotropic thermal expansion over the temperature range 300–700 K. $EuSO_4$ was examined by Raman, Fourier-transform infrared absorption and luminescence spectroscopy methods. $EuSO_4$ is found to be an indirect bandgap material with a bandgap close to direct electronic transition. The emission lifetime of divalent europium *d-f* emission in $EuSO_4$ shows an unusual behavior for stoichiometric compounds, as it shortens upon cooling from 1.11(1) μs at room temperature to 0.44(1) μs at 77 K.

Introduction

The chemistry of europium would be considered separately from the majority of the rare earth elements (REE), which is associated with the peculiarity of the *f*-sublevel filling. The half-filled f-sublevel causes europium to tend to a bivalent state. A similar tendency is also typical for Yb and Sm, which exhibit the stable compounds with an oxidation state of +2, but for which the redox potentials $E_{Ln(II/III)}$ are less favorite. Aqueous solutions with an oxidation state of +2 were found only for Sm, Eu, and Yb. This is due to the stability of $4f^7$ (Eu), $4f^{14}$ (Yb) shells, which are found in Ln^{2+} ions after the pinching off of the outer $6s^2$ electrons.[1–7] The reduction of $Eu^{3+} \rightarrow Eu^{2+}$ ions is used in the technology of separation of rare-earth raw materials.[7–14] Often, Eu^{2+} compounds possess very interesting luminescent,[15–17] catalytic[18,19] and magnetic properties.[20–22]

In terms of its properties, the Eu^{2+} ion is similar to analogous ions of alkaline earth metals[13] and, in particular, strontium because of almost identical ionic radii ($r(Eu^{2+}) = 0.112$ nm, $r(Sr^{2+}) = 0.127$ nm).[23] In the divalent state, europium mainly forms binary compounds, as well as compounds with complex non-oxidizing ions. In the structure of crystalline

[a] *Y. G. Denisenko*
Department of General and Special Chemistry,
Industrial University of Tyumen
Tyumen 625000, Russia
E-mail: yu.g.denisenko@gmail.com
[b] *Y. G. Denisenko, A. E. Sedykh, Prof. Dr. K. Müller-Buschbaum*
Institute of Inorganic and Analytical Chemistry,
Justus-Liebig-University of Giessen
35392 Giessen, Germany
[c] *Y. G. Denisenko, N. O. Azarapin, Dr. E. I. Sal'nikova, Prof. Dr. O. V. Andreev, Prof. Dr. I. A. Razumkova*
Department of Inorganic and Physical Chemistry,
Tyumen State University
Tyumen 625003, Russia
[d] *Dr. A. S. Oreshonkov*
Laboratory of Molecular Spectroscopy,
Kirensky Institute of Physics,
Federal Research Center KSC SB RAS
Krasnoyarsk 660036, Russia
[e] *Dr. A. S. Oreshonkov*
School of Engineering and Construction,
Siberian Federal University
Krasnoyarsk 660041, Russia
[f] *Dr. M. S. Molokeev*
Institute of Engineering Physics and Radioelectronics,
Siberian Federal University
Krasnoyarsk 660041, Russia
[g] *Dr. M. S. Molokeev*
Laboratory of Crystal Physics,
Kirensky Institute of Physics,
Federal Research Center KSC SB RAS
Krasnoyarsk 660036, Russia
[h] *Dr. M. S. Molokeev*
Research and Development Department,
Kemerovo State University
Kemerovo, 650000, Russia
[i] *Dr. E. I. Sal'nikova*
Research Department,
Northern Trans-Ural Agricultural University
Tyumen, 625003, Russia
[j] *Dr. O. D. Chimitova*
Baikal Institute of Nature Management,
SB RAS
Ulan-Ude, 670047, Russia
[k] *Prof. Dr. O. V. Andreev*
Laboratory of the Chemistry of Rare Earth Compounds,
Institute of Solid State Chemistry, UB RAS
Ekaterinburg, 620137, Russia
[l] *Prof. Dr. K. Müller-Buschbaum*
Center for Materials Research (LaMa),
Justus-Liebig-University of Giessen
Heinrich-Buff-Ring 16, 35392 Gießen, Germany

Supporting information for this article is available on the WWW under https://doi.org/10.1002/ejic.202200043

Research Article
doi.org/10.1002/ejic.202200043

hydrates, the Eu^{2+} ion is easily oxidized by presented crystalline hydrate water. For the same reason, aqueous solutions of halides are unstable. The introduction of chelating agents into aqueous solutions promotes the stability of the divalent state.[24–30] Europium (II) sulfate $EuSO_4$ is the most interesting from the point of view of materials, since it exhibits an increased stability,[31] most likely due to the chelating effect of the sulfate ion, which is often the case in europium sulfates of various compositions.[32–36]

A small number of methods for producing europium (II) sulfate is described in the literature, such as a synthesis method based on the reduction of europium (III) sulfate at a temperature of 500 °C. The disadvantage of this method is the necessity of a strict control of temperature in the synthesis zone, since even a slight excess of it will instantly lead to the formation of a by-product of the reaction, Eu_2O_2S.[37]

Europium (II) sulfate is formed as a result of reduction of a solution of europium (III) chloride in a Jones reducer on zinc amalgam in sulfuric acid under inert conditions.[38–43] A disadvantage of this method is the participation of doubly charged zinc ions in the process, which potentially enables the possibility of an isovalent substitution in the crystal structure of $EuSO_4$.

It is also possible to obtain $EuSO_4$ in the process of photochemical transformations, under the action of ultraviolet radiation, in solutions containing Eu^{3+} cations and SO_4^{2-} and HSO_4^- anions. The reactions are carried out either in an aqueous medium or in organic solvents: isopropyl formate, methanoic acid.[13,14,44–46] The disadvantage of the photochemical method is the duration of the process and rather low yields of the target product.

As can be seen, many methods for the synthesis of europium (II) sulfate are based on the use of europium (III) compounds. This fact in most cases does not allow achieving the required product purity or takes a long time. The development of methods for the synthesis of europium (II) sulfate using stable europium (II) compounds as starting materials is an urgent trend in the field of inorganic chemistry.

All of the above determines the relevance of the development of new and highly efficient methods for the synthesis of europium (II) sulfate and the study of its fundamental structural and physicochemical properties.

Results and Discussions

The interaction of europium sulfide EuS with aqueous solutions **(Method 1)** of sulfuric acid proceeds according to the equation (1):

$$EuS + H_2SO_4 \rightarrow EuSO_4 + H_2S \uparrow \quad (1)$$

The complete conversion of starting materials into reaction products is facilitated by the removal of hydrogen sulfide from the reaction zone, which is one of the conditions for the reaction to proceed to the end. However, the process is rather slow. Time of reaction for a 0.5 g sample of EuS takes ~30 minutes.

The rate of interaction of sulfides with sulfuric acid is mainly influenced by two factors:

- formation in the course of the reaction of a hindering layer of insoluble compound on the surface of the particles
- structural difficulty associated with much greater symmetry and density of ball packing in the structure of europium monosulfide, compared, for example, with sesqui-sulfides of rare earth elements, which easily interact with aqueous solutions of acids.[47,48]

To reduce these factors, it was decided to carry out the reaction of sulfide powder with a 10% solution of H_2SO_4 when exposed to ultrasonic vibrations. Here, a weighted portion of europium monosulfide weighing 0.50 g was placed in a beaker and a small amount of water was added so that it moistened all the monosulfide. The beaker was then placed in an ultrasonic bath filled with water, after which the acid solution was carefully added. It was found that the interaction proceeds much faster in the environment of ultrasonic vibrations. Time of reaction about 2 minutes for the sample.

According to X-ray phase analysis, the white-colored polycrystalline products of the reaction of europium monosulfide with sulfuric acid are powders of europium (II) sulfate $EuSO_4$ (Figure S1a,b). The reflections in the diffraction patterns are significantly broadened and have a low intensity. Full-profile refinement of diffraction patterns gives approximately the same crystallite size in both cases, being ~19 nm. According to the data of scanning electron microscopy, both samples are finely dispersed and consist of particles of a size mainly up to 1 μm (Figure 1a, Figure 1b). However, in the case of a sample obtained under the action of ultrasonic vibrations, the particle size is, on average, five times smaller.

The method based on the precipitation of europium sulfate from an aqueous solution **(Method 2)** can be described by the equation (2) and equation (3):

$$I) EuS + 2HCl \rightarrow EuCl_2 + H_2S \uparrow \quad (2)$$

$$II) EuCl_2 + H_2SO_4 \rightarrow EuSO_4 \downarrow + 2HCl \quad (3)$$

Chemical homogenization associated with the conversion of europium ions Eu^{2+} into a soluble form and the subsequent precipitation of europium sulfate, leads to the formation of more crystalline powders, although it requires two stages. A sample of europium (II) sulfate obtained by precipitation from a chloride solution, according to X-ray diffraction data, shows high crystallinity (Figure S1c). According to electron microscopy data, the powder is formed mainly by particles ranging in size from 1 to 2 μm (Figure 1c). In particles of an irregular round shape, an octahedral motif is often found.

Space group and unit cell parameters of europium sulfate were reported earlier in the work.[38] However, to date, there is no detailed analysis of the crystal structure. In particular, the coordinates of the atoms have not been determined and a detailed analysis of their coordination environment has not been performed. The vibrational properties of the structure

Research Article
doi.org/10.1002/ejic.202200043

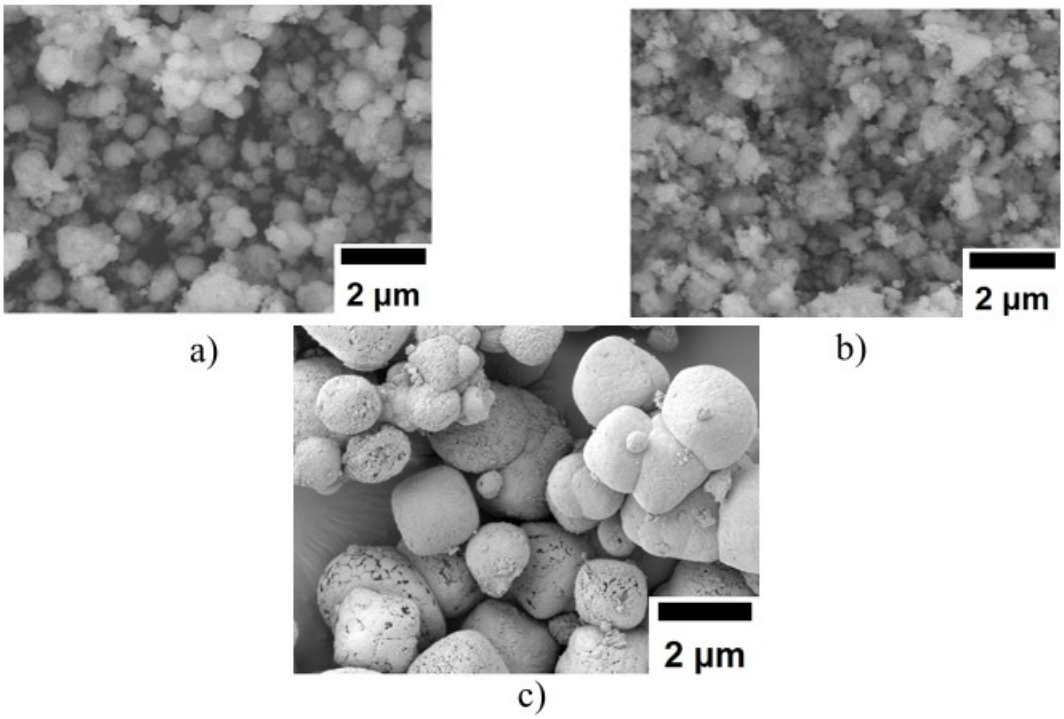

Figure 1. SEM images of particles obtained by method I: without ultrasonic (a) and with ultrasonic (b); and according by method II (c).

were also not discussed. According to powder X-ray diffraction data, all reflections are indexed by an orthorhombic cell (*Pnma*) with parameters close to $SrSO_4$.[49] Therefore, this structure was taken as the starting model for Rietveld refinement, which was performed using TOPAS 4.2.[50] The site of Sr^{2+} ion was occupied by an Eu^{2+} ion. The thermal parameters of Eu^{2+} and S^{6+} ions were refined anisotropically (Table S1), and thermal parameters of all O^{2-} ions were refined isotropically. The refinement was stable and gave low *R*-factors (Table 1, Figure 2).

Coordinates of atoms and main interatomic distances are listed in Table S2 and Table S3, respectively. Additional nine powder patterns obtained at 300–700 K were also refined using this structural model. It can be seen that all cell parameters a, b, c and volumes increase with heating, and the junction exhibits almost isotropic expansion (Figure 3, Table S4).

Table 1. Main parameters of processing and refinement of the $EuSO_4$ sample.

Compound	$EuSO_4$
Sp.Gr.	*Pnma*
a, Å	8.44264 (2)
b, Å	5.428433 (15)
c, Å	6.97537 (2)
V, Å^3	319.6834 (15)
Z	4
2θ-interval, °	5–140
R_{wp}, %	4.12
R_p, %	3.16
R_{exp}, %	2.39
χ^2	1.73
R_B, %	1.72

In the structure (Figure 4a), all europium atoms are eight-coordinate, forming bi-caped trigonal prism, and occupy identical crystallographic positions. Six sulfate groups bind to an europium ion monodentate, and one as chelate, resulting in the formation of a coordination polyhedron in the form of a double-capped trigonal prism. The chelating distances are significantly longer than the monodentate distances, resulting in a coordination number for europium of 6 + 2 (Figure 4b).

The double-capped trigonal prisms [EuO_8] are connected by edges in pairs to form zigzag chains along the *a*-direction (Figure 4c). In the b-direction, [EuO_8] eight vertices are linked to each other through the vertices of two sulfate polyhedra, forming a straight chain (Figure 4d). A similar mechanism of binding coordination polyhedra leads to the formation of a three-dimensional framework structure.

The infrared and Raman spectra of $EuSO_4$ are presented in Figure 5. Broad bands related to asymmetric stretching vibrations of $[SO_4]^{2-}$ ions observed in the regions of 1025–1250 cm^{-1}.[51] The sharp band at 990 cm^{-1} in the infrared spectrum and very strong band in the Raman spectrum at 994 cm^{-1} are representing symmetric stretching modes of the SO_4 tetrahedra.[52] Bands related to asymmetric bending modes observed in the region of 550–680 cm^{-1} in the infrared spectrum are in the range of 590–660 cm^{-1} in the Raman spectrum. Raman bands between 420 and 480 cm^{-1} are symmetric bending vibrations of sulfate ions. The lattice modes are located below 300 cm^{-1} with weak intensity.

The calculated band structure of $EuSO_4$ is demonstrated in Figure 6a. The path along high symmetry points of the Brillouin Zone (BZ) (Figure S2) was selected as: Γ-X-S-Y-Γ-Z-U-R-T-Z | X-U |

Research Article
doi.org/10.1002/ejic.202200043

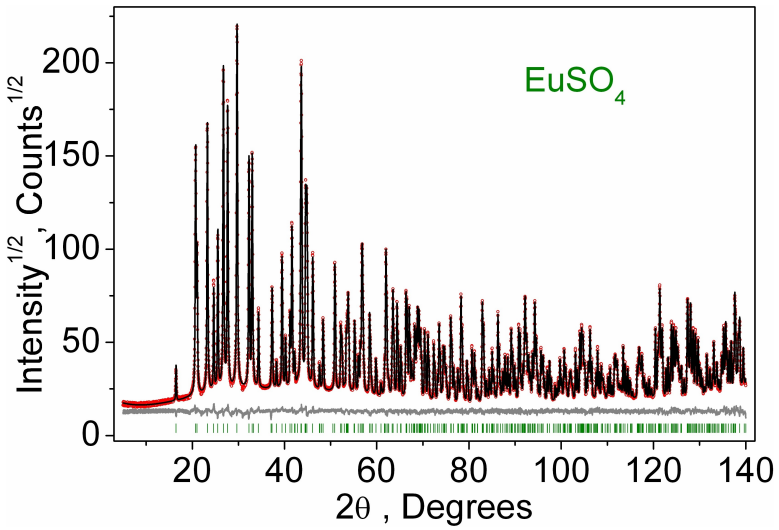

Figure 2. Difference Rietveld plot of $EuSO_4$.

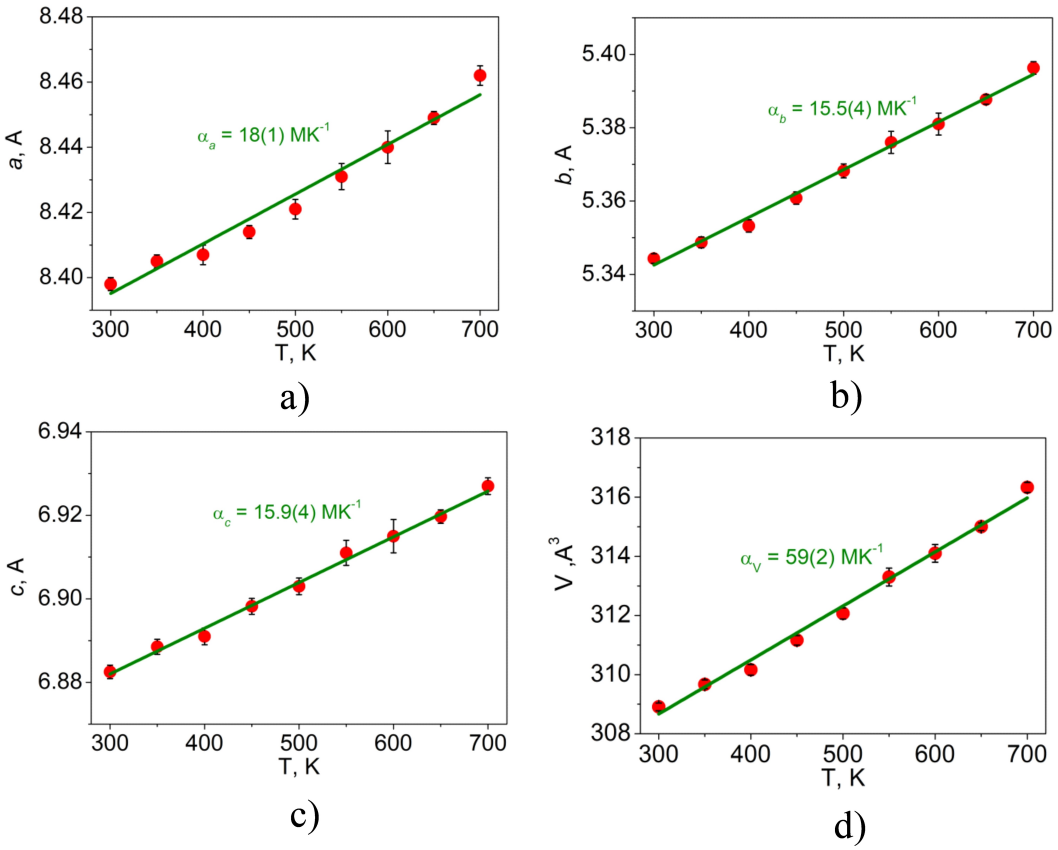

Figure 3. Cell parameters dependences per T: a) *a*(T); b) *b*(T); c) *c*(T); d) *V*(T).

Y-T|S-R.[53] Coordinates of these points are: Γ(0,0,0), X(0.5,0,0), S(0.5,0.5,0), Y(0,0.5,0), Z(0,0,0.5), U(0.5,0,0.5), R(0.5,0.5,0.5), T-(0,0.5,0.5). The value of the calculated bandgap was determined as the difference between the maximum of the valence band (MVB) and the minimum of the conduction band (MCB). As the europium ion is a lanthanide ion, the band structure presented has spin up and spin down components. The MCB is located at the center of the BZ, while the MVB is at the X point classifying $EuSO_4$ as an indirect bandgap material, although, the difference between indirect and direct transition is very small, as seen in Figure 5a. The experimental value of the bandgap was determined from the UV reflectance spectra using the Kubelka-

Research Article
doi.org/10.1002/ejic.202200043

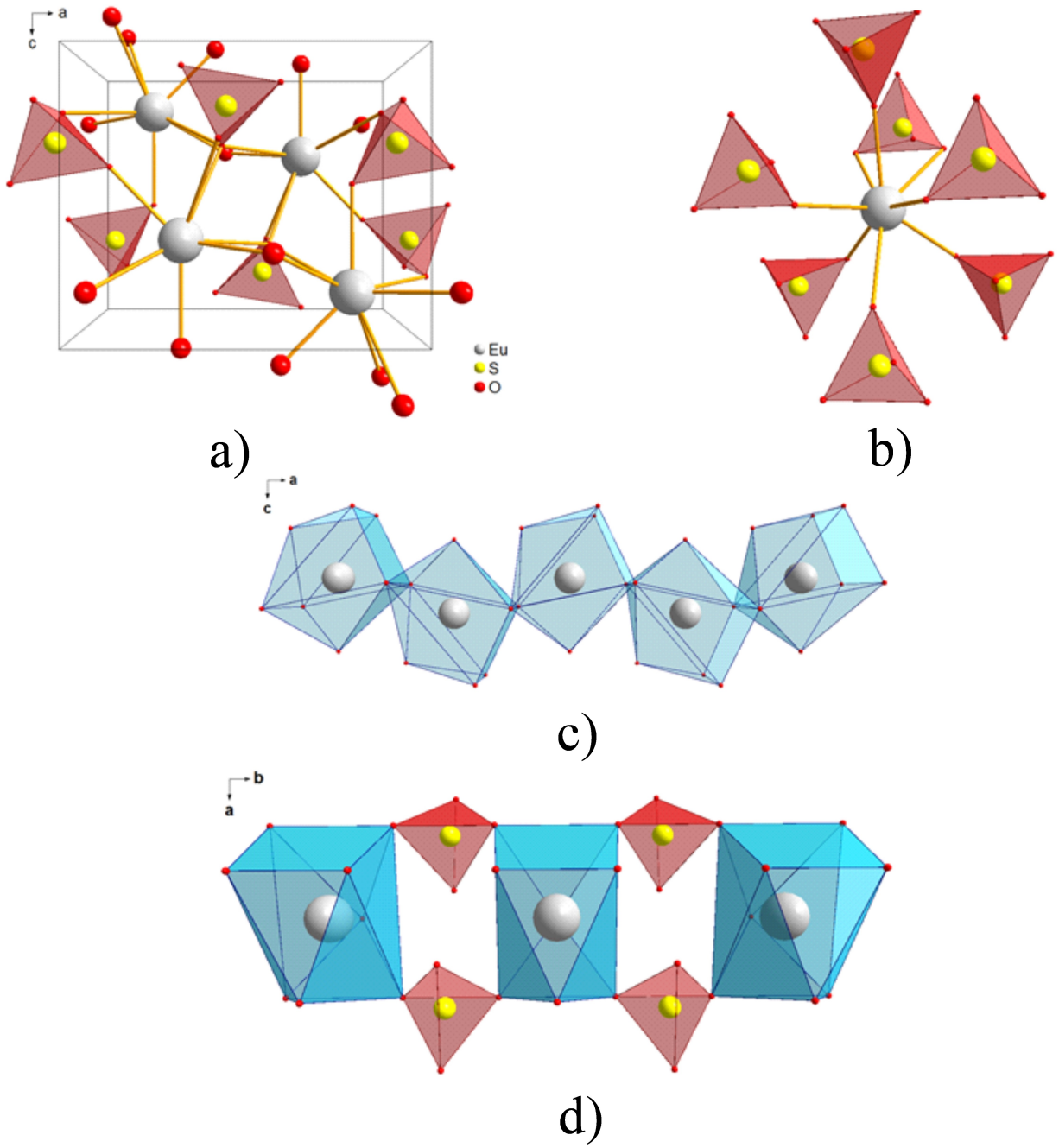

Figure 4. Perspective projection of the crystal structure (a), coordination of the Eu^{2+} ion (b), excerpt of one-dimensional chains $[EuO_8]_n$ (c), and $\{[EuO_8](SO_4)_2\}_n$ (d) in the structure of $EuSO_4$.

Munk equation: $Fl{=}K/S = (1\text{-}R)/2R$. Where K is the absorption coefficient, S is the scattering coefficient and R is the reflectance of material. The Tauc plot[54] is shown in Figure 6b, it shows the dependence of the Kubelka-Munk function $(Fl h\nu)^n$ on photon energy $h\nu$. The nature of the electronic transition (direct or indirect) can be determined by the exponent n (2 in case of direct and 1/2 in case of indirect electronic transition). As shown in Figure 6b, a linear extrapolation function to the abscissa axis is successful in case of $n = 2$, and the value of direct bandgap was determined as 4.32 eV. Calculated total electronic density of states (DOS) and partial DOS of $EuSO_4$ are shown in Figure 7. The results show that the Eu:4*f* states have a significant contribution near the Fermi level (MVB). The MCB is formed by contribution of d states of europium.

For Eu^{2+}, *d-f* luminescence depends on the coordination environment, unlike *f-f* luminescence of Eu^{3+}. In the excitation spectrum of $EuSO_4$ (Figure 8), a broad excitation band can be observed from 265 to 380 nm. At 77 K, $4f^6 5d \leftarrow 4f^7$ transitions become slightly distinct, alongside with *f-f* transition $^6P_{7/2} \leftarrow {}^8S_{7/2}$ at 360 nm. However, to thoroughly analyze these transitions,

Research Article
doi.org/10.1002/ejic.202200043

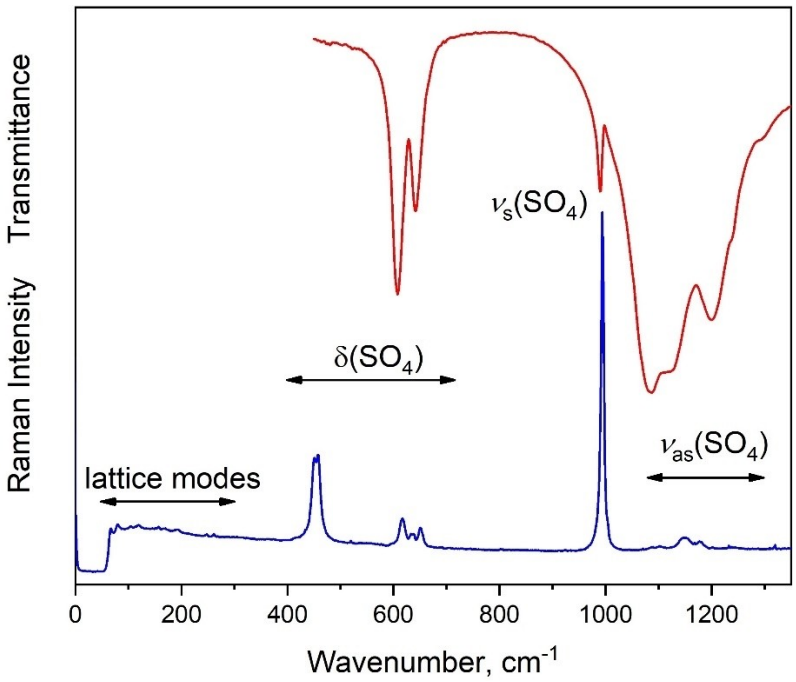

Figure 5. Infrared (red) and Raman (blue) spectra of $EuSO_4$.

one should typically investigate Eu^{2+} samples at temperatures of 4–10 K.[55,56] In the emission spectra, at both, room temperature and 77 K, a single broad band emission in the ultraviolet region can be observed (Figure 8). Maximum of the emission is 379 nm at room temperature and 382 nm at 77 K. At low temperature, the emission band is slightly narrower, due to the lower thermal vibrations in the structure. The qualitative luminescence behavior of investigated stoichiometric compound is similar to previously described isostructural $SrSO_4$:Eu^{2+} (0.2 mol%) at both, RT and 77 K.[57]

In order to further analyze the processes involved, also a determination of luminescence lifetimes was conducted (Figure 9). The overall emission intensity decay times were measured at both temperatures (RT and 77 K) using pulsed diode with a maximum wavelength of 290 nm as excitation source. The overall emission intensity decay of $EuSO_4$ cannot be described as a monoexponential decay at both temperatures, however, the decay remains the same over the whole emission profile. At room temperature, the emission intensity decay can be described with a three exponential decay with an average lifetime is 1.11(1) μs (Figure S4 and Table S3). At 77 K, the decay can be fitted with two exponential decay function with an average lifetime being shorter, namely 0.44(1) μs (Figure S4 and Table S5).

Such an unusual behavior of an emission lifetime shortening upon cooling was observed before for Eu^{2+}-doped materials, with two models being discussed.[56,58–64] According to Spoonhower and Burberry,[59] if the emissive $4f^65d$ excited states are high in energy and close to the excited $4f^7$ state ($^6P_{7/2}$) at around 27600 cm^{-1},[64] at higher temperature, the latter is thermally populated which leads to the extended observed lifetime of the emission, as the *f–f* transitions are forbidden. Meijerink and Blasse describe a second possible mechanism: in systems with small exchange interaction with the coordination environment, splitting between $4f^65d$ octet and sextet energy levels is small. This leads to a higher thermal population of energetically higher sextet energy levels at elevated temperatures, and as the transition between this state and the $^8S_{7/2}$ (octet) ground state is spin-forbidden, which leads to an increase of the emission lifetime.[56] For $EuSO_4$, both mechanisms can play a role, which may explain the polyexponential character of overall emission intensity decay as well as the longer average lifetime at a higher temperature. To the best of our knowledge, this phenomenon was not reported before for a stoichiometric divalent europium compound.

Conclusion

$EuSO_4$ was obtained from EuS by two independent methods: by direct interaction with concentrated sulfuric acid and through the intermediate product $EuCl_2$. The variations in the synthesis method affect the rate of interaction and the concentration of sulfuric acid, which is required for total conversion of EuS to $EuSO_4$. Based on the use of a stable starting compound containing Eu^{2+} ions, the presented methods make it possible to obtain a product with a high degree of purity in a fairly short time. This is mainly due to the absence of kinetic hindrances in the reduction of the Eu^{3+} ion, which occurs in all the methods described earlier. Complete conversion of the starting compound into the target product provides a high yield for the reaction. The compound $EuSO_4$ was systematically investigated.

Research Article
doi.org/10.1002/ejic.202200043

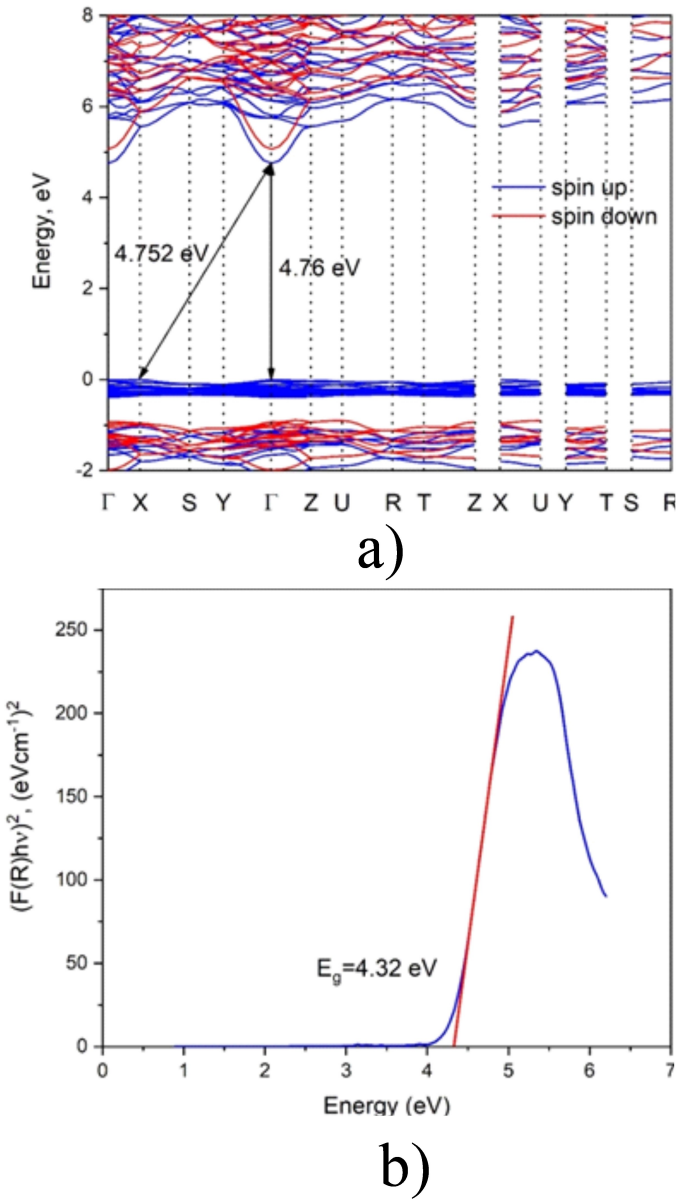

Figure 6. Electronic band structure (a) and UV-spectrum (b) of $EuSO_4$.

All europium atoms are eight-coordinate and occupy identical crystallographic positions in the structure of $EuSO_4$. The coordination environment of Eu^{2+} affects the *d-f* luminescence. In the excitation spectrum of $EuSO_4$, a broad excitation band is observed from 265 to 380 nm. In the emission spectra, a single broad band emission in the UV region can be observed with maximum of the emission is 379 nm at room temperature and 382 nm at 77 K. The data obtained are of fundamental importance and can be useful for researchers working with materials related to the divalent europium compound.

Experimental Section

Preparative methods

Synthesis of europium (II) sulfide EuS

Europium monosulfide EuS synthesized by the high-temperature reaction of europium oxide Eu_2O_3 with carbon disulfide vapor at a temperature of 1100 °C. Detailed synthesis parameters and the installation scheme are present in.[33]

Argon gas at a rate of 6 L/h passed through a glass round bottom flask with carbon disulfide heated to 40 °C in a heating mantle. First, an argon flow with CS_2 vapor was passed through a vertical quartz reactor loaded with europium oxide (m = 10 g) at room temperature for 30 min. Then, using a programmable controller, the temperature in the vertical oven increased to 1100 °C at a rate of 50 °C/min. After that, the process carried out at the specified parameters for 5 h. The polycrystalline product thus obtained has the stoichiometric composition EuS and does not contain impurities (Figure S4).

Synthesis methods of europium sulfate (II) $EuSO_4$

Method I. To obtain europium (II) sulfate, a reaction between EuS and H2SO4 used. For this, a weighted portion of europium sulfide was dispersed in deionized water, after which an equivalent amount of sulfuric acid solution (C = 14 mol/L) was added dropwise. After completion of the reaction, the liquid decanted from the precipitate and washed several times with distilled water, then filtered on a porous filter and dried in a desiccator over silica gel to constant weight. This reaction takes ~30 minutes to complete.

To reduce the time required for the reaction to proceed, it decided to conduct it in an environment of ultrasonic vibrations. Here for, a weighed portion of europium monosulfide weighing 0.50 g placed in a beaker and a small amount of water added so that it moistened all the monosulfide. The beaker then placed in an ultrasonic bath with a frequency of 35 kHz filled with water, after which the acid solution carefully added. It found that in the environment of ultrasonic vibrations, the interaction proceeds much faster. It took about 2 minutes for the sample to interact fully. The separation of the product from the mother liquor performed as described above.

Method II. To obtain europium sulfate by precipitation synthesis was carried out in two stages. At the first stage, a weighed portion of europium sulfide is dispersed in distilled water, after which, with constant stirring, concentrated hydrochloric acid (C = 12 mol/L) is added dropwise to the resulting suspension until the monosulfide is completely dissolved. Then to the resulting solution is added dropwise 2 N sulfuric acid in a volume exceeding 10% of the required equivalent. As a result, a white powder precipitated which decanted, washed several times with deionized water and dried in a desiccator over silica gel to constant weight.

In all methods, the yield of the target product is 98–99%. Insignificant losses are associated with filtration.

Analysis methods

The X-ray phase analysis (XRD) performed on a BRUKER D2 PHASER diffractometer with a linear detector LYNXEYE (CuKα radiation, Ni-filter). The Rietveld refinement of the selected six samples performed using package TOPAS 4.2.[50] The powder diffraction data of $EuSO_4$ for Rietveld analysis collected at room temperature with a Bruker D8 ADVANCE powder diffractometer (Cu–Kα radiation) and linear VANTEC detector. The step size of 2θ was 0.016° and the

Research Article
doi.org/10.1002/ejic.202200043

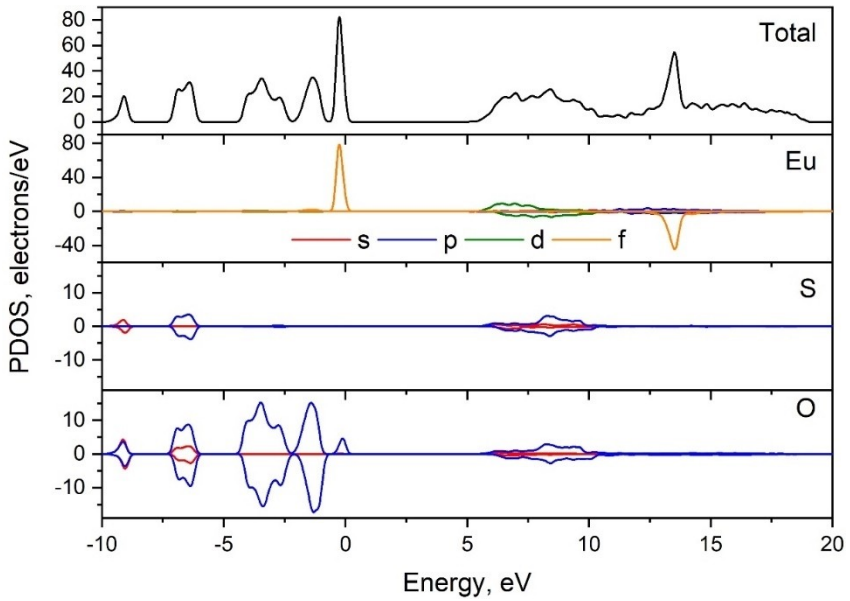

Figure 7. Density of states (DOS) and partial density of states (PDOS) of $EuSO_4$.

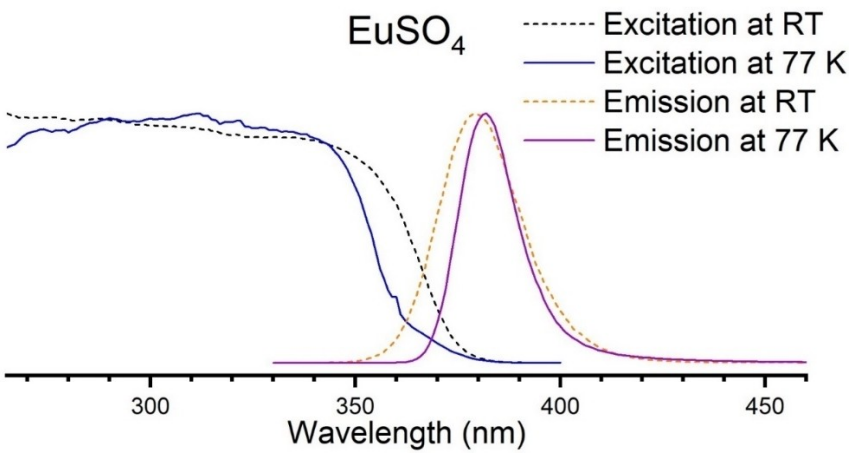

Figure 8. Excitation and emission spectra of $EuSO_4$.

counting time was 5 s per step. Additional nine XRD patterns measured in the temperature range of 300–700 K with the 50 K step using Rigaku D/MAX-2200VL/PC (Japan) diffractometer with Anton Paar heat attachment. The 2θ range of 10–60° measured with 0.6 mm divergence slit, the step size of 2θ was 0.02°, and the counting time was 0.4 s per step.

The crystallographic data are deposited in Cambridge Crystallographic Data Centre (CSD #2143152).

The electron-microscopy analysis carried out on an electron microscope JEOL JSM-6510LV. The X-ray energy-dispersive analyzer used to register the X-rays at the element spectrum plotting in selected sample surface areas. The element content determination inaccuracy in element content determination was equal to ±0.2%.

The Fourier-transform infrared spectroscopy (FTIR) analysis carried out on a Fourier Transform Infrared Spectrometer FSM 1201. The sample for the investigation was prepared in the tablet shape with the addition of annealed KBr. Raman spectra recorded using an i-Raman Plus spectrometer at a laser excitation wavelength of 785 nm.

For the photoluminescence investigations, the sample mortared, filled in a quartz glass cuvette, and examined at room temperature and at 77 K (using special liquid nitrogen-filled Dewar assembly). The spectra were recorded on a Horiba Jobin Yvon Spex Fluorolog 3 spectrophotometer equipped with a 450 W Xe short-arc lamp (USHIO), double-grated excitation and emission monochromators, a photomultiplier tube (R928P) and a TCSPC upgrade using the FluoroEssence software. Both, excitation and emission spectra corrected for the spectral response of the monochromators and detector using spectral corrections provided by the manufacturers. The excitation spectra corrected for the spectral distribution of the lamp intensity by use of a photodiode reference detector. The emission decays recorded with a pulsed diode with an excitation wavelength of 290 nm using the Data Station software (HORIBA DeldaDiode-290). Exponential tail fitting used for calculation of the resulting intensity decay using the Decay Analysis software. The

Research Article
doi.org/10.1002/ejic.202200043

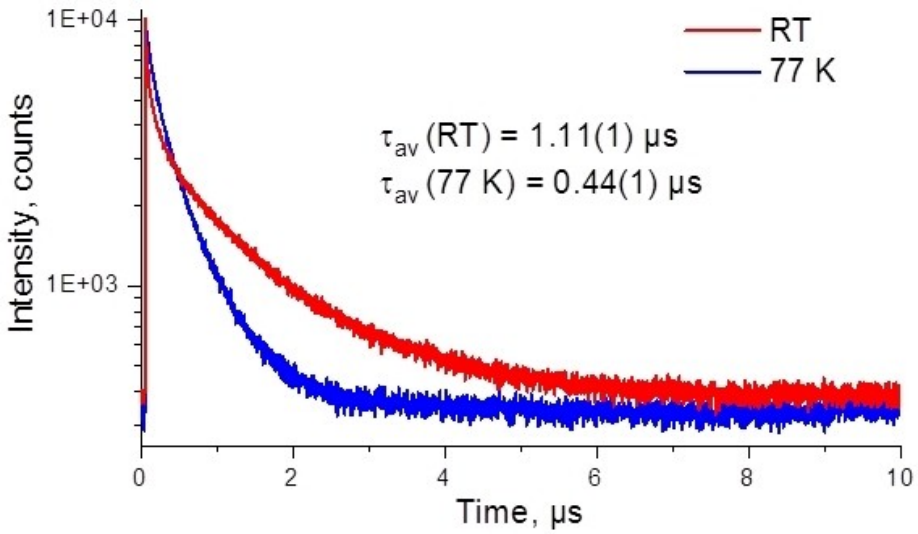

Figure 9. Comparison of overall emission intensity decays of $EuSO_4$ measured at RT and 77 K.

quality of each fit confirmed by χ2 value. Average lifetimes were calculated by two methods: as a mathematical average (Equation 4) and as a previously described in the literature equation for calculation of non-monoexponential emission lifetime (Equation 5)[65] – both results in similar values (see SI Table S5).

$$\tau_{av} = \frac{\sum_i B_i \cdot \tau_i^2}{\sum_i B_i \cdot \tau_i} \quad (4)$$

$$\tau_{av} = \frac{\int_0^\infty t \cdot I(t)dt}{\int_0^\infty I(t)dt} \quad (5)$$

The first-principles density functional theory calculations[66,67] performed using the CASTEP code (version 20.1.1).[68] The $4f^7 5\,s^2 5p^6 6\,s^2$, $3\,s^2 3p^4$ and $2\,s^2 2p^4$ valence electron configurations used for Eu, S and O, respectively. The electron-electron exchange-correlation functional was treated using the Generalized Gradient Approximation parametrized by Perdew, Burke and Ernzerhof.[69] The on-the-fly-generated norm-conserving pseudopotentials used and the cutoff energy of 1370 eV for the plane-wave basis set was used. The Γ-centered 2×4×3 k-point mesh[70] used.

Deposition Number 2143152 (for $EuSO_4$) contains the supplementary crystallographic data for this paper. These data are provided free of charge by the joint Cambridge Crystallographic Data Centre and Fachinformationszentrum Karlsruhe Access Structures service www.ccdc.cam.ac.uk/structures.

Acknowledgement

This research is partially supported by the state order of BINM SB RAS (project no. 0273-2021-0008). Open Access funding enabled and organized by Projekt DEAL.

Conflict of Interest

The authors declare no conflict of interest.

Data Availability Statement

Research data are not shared.

Keywords: Europium · Inorganic synthesis · Luminescence · Structure elucidation · Sulfates

[1] N. N. Greenwood, A. Earnshaw, *Elsevier* **2012**.
[2] D. F. Shriver, P. W. Atkins, *Oxford University Press* **2010**.
[3] F. Nief, *Dalton Trans.* **2010**, *39*, 6589–6598.
[4] D. O. Khristolyubov, D. M. Lyubov, A. A. Trifonov, *Russ. Chem. Rev.* **2021**, *90*, 529.
[5] T. C. Jenks, M. D. Bailey, J. L. Hovey, S. Fernando, G. Basnayake, M. E. Cross, W. Li, M. J. Allen, *Chem. Sci.* **2018**, *9*, 1273–1278.
[6] T. P. Gompa, N. Jiang, J. Bacsa, H. S. La Pierre, *Dalton Trans.* **2019**, *48*, 16869–16872.
[7] R. Yadav, T. Simler, M. T. Gamer, R. Köppe, P. W. Roesky, *Chem. Commun.* **2019**, *55*, 5765–5768.
[8] J. A. Rard, *J. Solution Chem.* **1988**, *17*, 499–517.
[9] T. Hirai, I. Komasawa, *J. Chem. Eng. Jpn.* **1992**, *25*, 644–648.
[10] S. A. Sayed, K. A. Rabie, I. E. Salama, *Sep. Purif. Technol.* **2005**, *46*, 145–154.
[11] C. A. Morais, V. S. Ciminelli, *Miner. Eng.* **2007**, *20*, 747–752.
[12] A. Yörükoğlu, I. Girgin, *Hydrometallurgy* **2002**, *63*, 85–91.
[13] S. Tsushima, S. Nagasaki, A. Suzuki, *J. Photochem. Photobiol. A* **1997**, *106*, 57–60.
[14] D. Nishida, M. Kusaba, T. Yatsuhashi, N. Nakashima, *Chem. Phys. Lett.* **2008**, *465*, 238–240.
[15] A. Akella, D. A. Keszler, *Chem. Mater.* **1995**, *7*, 1299–1302.
[16] Z. Fang, H. Yu, B. Zhang, D. Jiang, Q. Wu, L. Xiong, H. Zhao, L. Su, *J. Lumin.* **2021**, *233*, 117877.
[17] F. Su, B. Lou, Y. Ou, Y. Yang, W. Zhou, C.-K. Duan, H. Liang, *J. Phys. Chem. C.* **2021**, *125*, 5957–5967.
[18] M. Zhang, F. Li, S. Jiang, Y. C. Lin, F. Chen, X. Zhao, Y. Shen, *Opt. Mater.* **2021**, *116*, 111049.
[19] W. Ye, Q. Huang, X. Liu, G. Hu, *Acta Mater.* **2017**, *122*, 420–430.
[20] T. Terashima, N. Kurita, A. Kikkawa, H. S. Suzuki, T. Matsumoto, K. Murata, S. Uji, *J. Phys. Soc. Jpn.* **2010**, *79*, 103706.
[21] J. Garcia, A. N. Kuda-Wedagedara, M. J. Allen, *Eur. J. Inorg. Chem.* **2012**, *12*, 2135–2140.
[22] I. V. Plokhikh, N. Khan, A. A. Tsirlin, A. N. Kuznetsov, D. O. Charkin, A. V. Shevelkov, A. Pfitzner, *Inorg. Chem. Front.* **2020**, *7*, C, 1115–1126.

[23] R. D. Shannon, *Acta Crystallogr. Sect. A* **1976**, *32*, 751–767.
[24] E. A. Mironov, O. V. Palashov, D. N. Karimov, *Scr. Mater.* **2019**, *162*, 54–57.
[25] S. Batygov, M. Brekhovskikh, L. Moiseeva, I. Zhidkova, S. Yurtaeva, *J. Non-Cryst. Solids* **2018**, *480*, 57–60.
[26] S. Kolenda, C. Sürgers, G. Fischer, D. Beckmann, *Phys. Rev. B* **2017**, *95*, 224505.
[27] W. Boncher, H. Dalafu, N. Rosa, S. Stoll, *Coord. Chem. Rev.* **2015**, *289*, 279–288.
[28] D. F. Evans, G. V. Fazakerley, R. F. Phillips, *J. Chem. Soc. A* **1971**, 1931–1934.
[29] Z. Bai, B. Gong, Y. Tian, Q. Zhang, C. Song, *J. Chin. Ceram. Soc.* **2008**, *36*, 1753–1757.
[30] G. Heckmann, M. Niemeyer, *J. Am. Chem. Soc.* **2000**, *122*, 4227–4228.
[31] Y. G. Denisenko, N. A. Khritokhin, O. V. Andreev, S. A. Basova, E. I. Sal'nikova, A. A. Polkovnikov, *J. Solid State Chem.* **2017**, *255*, 219–224.
[32] Y. G. Denisenko, A. S. Aleksandrovsky, V. V. Atuchin, A. S. Krylov, M. S. Molokeev, A. S. Oreshonkov, N. P. Shestakov, O. V. Andreeva, *J. Ind. Eng. Chem.* **2018**, *68*, 109–116.
[33] Y. G. Denisenko, M. S. Molokeev, A. S. Krylov, A. S. Aleksandrovsky, A. S. Oreshonkov, V. V. Atuchin, N. O. Azarapin, P. E. Plyusnin, E. I. Sal'nikova, O. V. Andreev, *J. Ind. Eng. Chem.* **2019**, *79*, 62–70.
[34] Y. G. Denisenko, A. E. Sedykh, M. S. Molokeev, A. S. Oreshonkov, A. S. Aleksandrovsky, A. S. Krylov, N. A. Khritokhin, E. I. Sal'nikova, O. V. Andreev, K. Müller-Buschbaum, *J. Solid State Chem.* **2021**, *294*, 121898.
[35] S. J. Park, M. H. Joo, S.-M. Hong, J.-G. Kang, C. K. Rhee, S. W. Lee, Y. Sohn, *Inorg. Chem. Front.* **2021**, *8*, 1175–1188.
[36] S. J. Park, M. H. Joo, S.-M. Hong, C. K. Rhee, J.-G. Kang, Y. Sohn, *Chem. Eng. J.* **2021**, *412*, 128717.
[37] O. V. Andreev, Y. G. Denisenko, E. I. Sal'nikova, N. A. Khritokhin, K. S. Zyryanova, *Russ. J. Inorg. Chem.* **2016**, *61*, 296–301.
[38] I. Mayer, E. Levy, A. Glasner, *Acta Crystallogr.* **1964**, *17*, 1071–1072.
[39] C. A. Morais, V. S. T. Ciminelli, *Hydrometallurgy* **1998**, *49*, 167–177.
[40] H. W. Stone, D. N. Hume, *Ind. Eng. Chem. Anal. Ed.* **1939**, *11*, 598–602.
[41] B. Kronholm, C. G. Anderson, P. R. Taylor, *JOM* **2013**, *65*, 1321–1326.
[42] Y. Takahashi, G. R. Kolonin, G. P. Shironosova, I. I. Kupriyanova, T. Uruga, H. Shimizu, *Mineral. Mag.* **2005**, *69*, 179–190.
[43] E. Lagendijk, F. J. A. M. Greidanus, H. W. J. Blöte, *Physica B+C* **1977**, *92*, 369–372.
[44] M. Kusaba, N. Nakashima, Y. Izawa, C. Yamanaka, W. Kawamura, *Chem. Phys. Lett.* **1994**, *221*, 407–411.
[45] M. Kusaba, N. Nakashima, W. Kawamura, Y. Izawa, C. Yamanaka, *Chem. Phys. Lett.* **1992**, *197*, 136–140.
[46] C. A. de Morais, V. S. T. Ciminelli, *Sep. Sci. Technol.* **2002**, *37*, 3305–3321.
[47] I. A. Razumkova, Y. G. Denisenko, A. N. Boyko, D. A. Ikonnikov, A. S. Aleksandrovsky, N. O. Azarapin, O. V. Andreev, *Z. Anorg. Allg. Chem.* **2019**, *645*, 1393–1401.
[48] I. A. Razumkova, A. N. Boiko, O. V. Andreev, S. A. Basova, *Russ. J. Inorg. Chem.* **2017**, *62*, 418–422.
[49] K. Burger, D. Cox, R. Papoular, W. Prandl, *J. Appl. Crystallogr.* **1998**, *31*, 789–797.
[50] Bruker. *TOPAS V4: General Profile and Structure Analysis Software for Powder Diffraction Data-User's Manual.* **2008**.
[51] Y. G. Denisenko, M. S. Molokeev, A. S. Oreshonkov, A. S. Krylov, A. S. Aleksandrovsky, N. O. Azarapin, O. V. Andreev, I. A. Razumkova, V. V. Atuchin, *Crystals* **2021**, *11*, 1027.
[52] S. Grishina, S. Goryainov, A. Oreshonkov, N. Karmanov, *J. Raman Spectrosc.* **2021**, *53*, 497–507.
[53] Y. Hinuma, G. Pizzi, Y. Kumagai, F. Oba, I. Tanaka, *Comput. Mater. Sci.* **2017**, *128*, 140–184.
[54] J. Tauc, *Mater. Res. Bull.* **1968**, *3*, 37–46.
[55] Z. Pan, L. Ning, B.-M. Cheng, P. A. Tanner, *Chem. Phys. Lett.* **2006**, *428*, 78–82.
[56] A. Meijerink, G. Blasse, *J. Lumin.* **1990**, *47*, 1–5.
[57] N. Yamashita, I. Yamamoto, K. Ninagawa, T. Wada, Y. Yamashita, Y. Nakao, *Jpn. J. Appl. Phys.* **1985**, *24*, 1174–1180.
[58] P. Kisliuk, H. H. Tippins, C. A. Moore, S. A. Pollack, *Phys. Rev.* **1968**, *171*, 336–342.
[59] J. P. Spoonhower, M. S. Burberry, *J. Lumin.* **1989**, *43*, 221–226.
[60] C. K. Duan, A. Meijerink, R. J. Reeves, M. F. Reid, *J. Alloys Compd.* **2006**, *408–412*, 784–787.
[61] M. Tyagi, M. Zhuravleva, C. L. Melcher, *J. Appl. Phys.* **2013**, *113*, 203504.
[62] M. Müller, T. Jüstel, *Dalton Trans.* **2015**, *44*, 10368–10376.
[63] L. Wu, X. Zhang, J. Yang, Y. Xu, H. Zhang, M. He, G. Yuan, H. Jin Seo, *J. Lumin.* **2017**, *192*, 616–619.
[64] M. C. Downer, C. D. Cordero-Montalvo, H. Crosswhite, *Phys. Rev. B* **1983**, *28*, 4931–4943.
[65] M. Daldosso, D. Falcomer, A. Speghini, P. Chigna, M. Bettinelli, *Opt. Mater.* **2008**, *30*, 1162–1167.
[66] P. Hohenberg, W. Kohn, *Phys. Rev.* **1964**, *136*, B864–B871.
[67] W. Kohn, L. J. Sham, *Phys. Rev.* **1965**, *140*, A1133–A1138.
[68] S. J. Clark, M. D. Segall, C. J. Pickard, P. J. Hasnip, M. I. J. Probert, K. Refson, M. C. Payne, *Z. Kristallogr.* **2005**, *220*, 567–570.
[69] J. P. Perdew, K. Burke, M. Ernzerhof, *Phys. Rev. Lett.* **1996**, *77*, 3865–3868.
[70] H. J. Monkhorst, J. D. Pack, *Phys. Rev. B.* **1976**, *13*, 5188–5192.

Manuscript received: January 19, 2022
Revised manuscript received: March 1, 2022